Suppression of coffee ring: (Particle) size matters

Lalit Bansal, Pranjal Seth, Bhubesh Murugappan, and Saptarshi Basu

Citation: Appl. Phys. Lett. **112**, 211605 (2018); doi: 10.1063/1.5034119
View online: https://doi.org/10.1063/1.5034119
View Table of Contents: http://aip.scitation.org/toc/apl/112/21
Published by the American Institute of Physics

Suppression of coffee ring: (Particle) size matters

Lalit Bansal, Pranjal Seth, Bhubesh Murugappan, and Saptarshi Basu[a)]
Department of Mechanical Engineering, Indian Institute of Science, Bangalore 560012, India

(Received 9 April 2018; accepted 15 May 2018; published online 24 May 2018)

Coffee ring patterns in drying sessile droplets are undesirable in various practical applications. Here, we experimentally demonstrate that on hydrophobic substrates, the coffee ring can be suppressed just by increasing the particle diameter. Particles with larger size flocculate within the evaporation timescale, leading to a significant gravimetric settling (for $Pe > 1$) triggering a uniform deposit. Interestingly, the transition to a uniform deposit is found to be independent of the internal flow field and substrate properties. Flocculation of particles also alters the particle packing at the nanoscale resulting in order to disorder transitions. In this letter, we exhibit a physical exposition on how particle size affects morphodynamics of the droplet drying at macro-nano length scales. *Published by AIP Publishing*. https://doi.org/10.1063/1.5034119

Solvent evaporation induced particle self-assembly in functional droplets has been a topic of active research for decades cutting across multiple industries. A complete understanding of the process can help in effective tuning of the final morphology to cater to a wide range of applications. The applications include ink-jet printing,[1–3] DNA microarray,[4,5] photonic crystals,[6,7] micropatterning,[8–10] to name a few. The most commonly observed pattern in the field of colloidal droplet evaporation is the "coffee ring stain." Deegan *et al.*[11] were the first group to explain the physics responsible for coffee stains. They reported capillary driven particle transport to the pinned contact line to be the driving mechanism. However, many applications require uniform deposit instead of a ring one. There have been many attempts to suppress the coffee ring formation using various stimuli. Yunker *et al.*[12] used ellipsoidal particles instead of spherical ones affecting the long-ranged particle interactions. Li *et al.*[13] accelerated the evaporation dynamics by heating the droplet. This resulted in particle accumulation at the air-water interface instead of the contact line, thereby eliminating the coffee ring. Kajiya *et al.*[14] and Still *et al.*[15] added a surfactant to the colloidal suspension. This transformed the internal flow from capillary to Marangoni affecting the particle transport to the droplet edge. On the other hand, Hu and Larson[16] replaced the solvent from water to octane to induce Marangoni flow. All these aforementioned studies either used external stimuli such as surfactants which can be toxic[12] or modified the particle shape which can be time consuming and costly to manufacture. Moreover, all these works were done for hydrophilic conditions.

In the present work, we report the formation of coffee rings for high contact angle (CA) droplet (contact angle $> 90°$) and uniform deposit for low contact droplet (contact angle $< 90°$; for particle concentration of 1 wt. %), contrary to established intuitions. Such precipitates were formed even though the flow was neither capillary nor Marangoni in either of the cases. We present a physics-based methodology to obtain uniform coating on hydrophobic substrates just by increasing the particle size without changing the solvent, flow dynamics, and addition of surfactants. Here, we use spherical polystyrene particles (rhodamine coated polystyrene particles, Sigma Aldrich) of sizes, 50 nm, 200 nm, 520 nm, and 860 nm suspended in deionized water. Experiments are conducted for two droplet volumes (1 μl and 3 μl), with three initial particle loading rates (PLRs; 0.01, 0.1, and 1 wt. %) on two substrates: polydimethylsiloxane (PDMS; $R_a = 40$ nm) and gas diffusion layer (GDL; $R_a = 10\ \mu$m), where R_a is the surface roughness (see supplementary material for experimental methodology). To explain the transition from coffee ring to uniform deposit, only the extreme size of the particles, i.e., 50 nm (forms ring like deposits) and 860 nm (forms a more uniform pattern), at an initial PLR of 1 wt. % and initial volume of 3 μl, is discussed for brevity. We also conducted experiments on other rigid substrates like silicon wafer and Teflon to further verify the observed transition (Fig. S1).

Figure 1 shows the transition in morphology of the final precipitate from the conventional coffee ring (a: 50 nm) to a uniform deposit (d: 860 nm) on both PDMS and GDL while the PLR is kept constant. It is observed that for 50 nm suspension, the edge of the precipitate is much thicker (τ) than the center, thus indicating a "coffee ring" $\left({}^{\tau_{edge}}/_{\tau_{center}} = 7.6\right)$, where τ_{edge} and τ_{center} are the final deposit heights at the deposit edge and center, respectively (Fig. 2). Similar deposit was observed by Bansal *et al.*[17] for droplets loaded (initial PLR of 1 wt. %) with 22 nm diameter silica nanoparticles. The ring thickness ratio decreases with an increase in particle size $\left({}^{\tau_{edge}}/_{\tau_{center}} = 6\right)$ for 200 nm particles (weak coffee ring) and approaches unity as the particle size is gradually increased to 520 nm and 860 nm, indicating a uniform deposit pattern. The morpho-dynamics of any precipitate resulting from drying of particle laden droplets can be altered by controlling (a) initial droplet wettability, (b) internal flow field, (c) contact line dynamics, and (d) inter-particle and particle-substrate interactions.

To begin with, let us first discuss the role of initial droplet wettability. Normally, a pure water droplet deployed on PDMS and GDL substrate subtends an initial contact angle (CA) of $\theta_i \sim 110°$ and $\theta_i \sim 125°$, respectively.[18] In the present work, we observe a decrease in the initial CA for both PDMS $(\sim 100°)$ and GDL $(\sim 120°)$ for droplets of 50 nm

a)Email: sbasu@iisc.ac.in

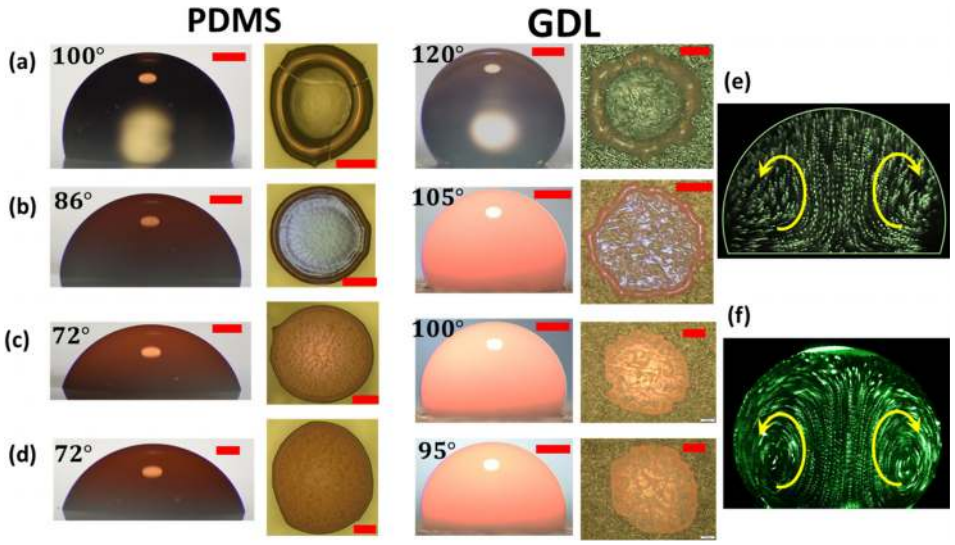

FIG. 1. Snapshots of droplets at deployment on PDMS and GDL and after complete evaporation for particle sizes (a) 50 nm, (b) 200 nm, (c) 520 nm, and (d) 860 nm. Particle loading rate is 1 wt. %. Numbers on the snapshots in first and third column denote the initial contact angle for that droplet. Images in third column show internal flow field (recirculatory toroidal pattern) for droplets evaporating on (e) PDMS and (f) GDL. PDMS and GDL are the polydimethylsiloxane and gas diffusion layer, respectively. Scale bar equals 200 μm. (e) and (f) Reproduced with permission from Appl. Phys. Lett. **111**, 101601 (2017). Copyright 2017 AIP Publishing LLC[26] and reproduced with permission from Bansal *et al.*, Phys. Rev. E **92**, 042304 (2015). Copyright 2015 American Physical Society, respectively.[27]

particle suspension at an initial concentration of 1 wt. % (Fig. 1). This is due to the fact that nanoparticles present at the interface and three-phase contact line change the solid-liquid and liquid-vapor interfacial tensions.[19–21] Moreover, surface tension is also affected by the particle size and number density. Thus, CA is further reduced to ∼70° and ∼95° for PDMS and GDL, respectively, as the particle size is increased from 50 nm to 860 nm while the PLR is kept constant. Thus, Fig. 1 indicates a correlation between initial contact angle change (50 nm–860 nm) and metamorphosis of the final deposit from ring to uniform pattern. However, the initial CA is found to increase as the initial PLR is reduced from 1 wt. % to 0.01 wt. % (Table S1). For the case of 860 nm particles, deposits from droplets on PDMS with low initial CA (∼70°) and high initial CA (∼100°) look very similar to each other $\left({}^{\tau_{edge}}/_{\tau_{center}} = 1\right)$. Similarly, for 50 nm droplets, the deposit is always ring like, irrespective of the initial CA. Thus, the transition from the ring to uniform deposit cannot be attributed to the initial CA. Although the correlation between particle dimensions (ellipsoidal particles) and the initial CA was previously reported by Yunker *et al.*,[12] even they attributed the suppression of coffee ring to the particle shape only and not to the change in the initial CA. The only discernable effect (Figs. 1 and S2) is the gradual decrease in the width of the ring for 50 nm droplet as the PLR is reduced to 0.01 wt. %.

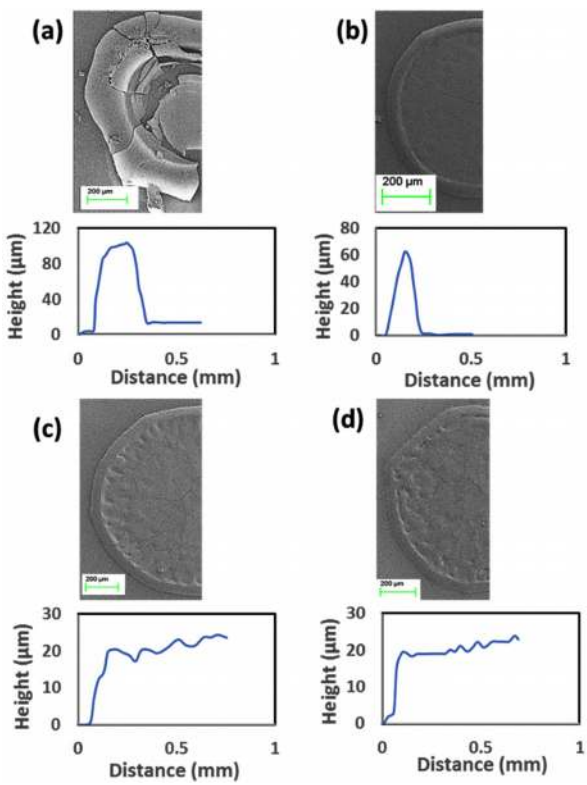

FIG. 2. SEM micrographs and corresponding optical profilometry data for (a) 50 nm, (b) 200 nm, (c) 520 nm, and (d) 860 nm for PDMS substrate showing ring to uniform deposit transition. Particle loading rate is 1 wt. %. Similar observations hold for GDL substrate also. Scale bar equals 200 μm.

The transition is found to be unaffected even by the change in the substrate property. As shown in Fig. 3, there is a marked difference in evaporating droplet's contact line dynamics on the two substrates. The deviation in the R/R_o profiles for the PDMS substrate has been explained in Fig. S3 (see caption). On PDMS, droplet evaporates initially in constant contact radius mode (CCR) $\left({}^{R_f}/_{R_o} = 0.4\right)$, where R_o and R_f are the initial and final contact radii, respectively, and then in constant contact angle (CCA) and finally in mixed mode. On the other hand, the only mode observed in the case of GDL (due to high surface roughness) is CCR $\left({}^{R_f}/_{R_o} = 0.9\right)$. Thus, it is expected that GDL will produce more pronounced coffee ring compared to PDMS due to the dominance of the CCR mode.[11] However, irrespective of the mode of evaporation, the 860 nm suspension always produces uniform deposits while the case of 50 nm results in ring deposits.

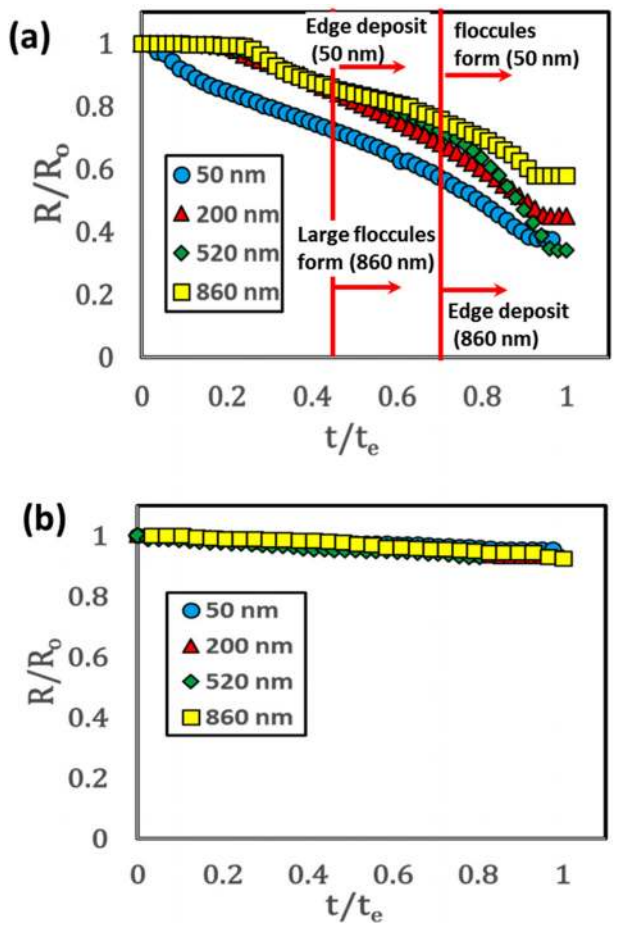

FIG. 3. Temporal variations in contact radius for (a) PDMS and (b) GDL for various particle sizes at particle loading rate of 1 wt. %. Error percent is 3%–5% standard deviation.

Next, we investigate the internal flow dynamics. The flow pattern in an evaporating droplet is usually driven by three known mechanisms. They are capillary driven, Marangoni driven, and buoyancy driven. As mentioned earlier, the capillary driven flow on hydrophilic substrates results in a coffee-ring shaped pattern.[11] On the other hand, the Marangoni driven flow suppresses the coffee ring.[15,16] However, on hydrophobic substrates, the internal flow is buoyancy driven recirculatory in nature[17,22] [Figs. 1(e) and 1(f)]. We found that the internal flow structure for all the cases reported (irrespective of substrate, PLR, and size) here are buoyancy driven toroidal (quantified using 860 nm particles at initial PLR of 0.008%; Stokes number $\ll 1$). Thus, similar flow patterns (toroidal) should have resulted in the same deposit topology for all the cases which is obviously not observed in the current experiments.

Thus, having eliminated initial droplet wettability, internal flow field, and modes of evaporation from the list of factors, we finally inspect the interactions between particle-particle and particle-substrate as plausible reason for transition. It is known that suspended particles experience van der Waals force of attraction as they come close to each other. Such interaction results in agglomeration forming larger floccules. These floccules are then circulated inside the droplet by the buoyancy driven toroidal flow. When they are closer to the substrate, they are attracted towards it due to the particle-substrate interaction (Fig. 4). van der Waals attractive force (W) increases with the particle size (r_p) as $W \propto r_p$.[23] This relation is true for both particle-particle and particle-substrate interactions. As a result, larger flocculates are formed for 860 nm particle suspension compared to 50 nm within the evaporation lifetime (t_e). Figure 5 shows the fluorescence images of the evaporating droplet dispersed with 50 nm and 860 nm particles. As the droplet evaporates, for 860 nm, particles start to agglomerate at $^t/_{t_e} > 0.5$ and large floccules ($\sim 30\,\mu\text{m} - 250\,\mu\text{m}$) are observed (Figs. 5 and S4). On the other hand, very few aggregates are visible at a similar phase $\left(\sim 5\,\mu\text{m at } ^t/_{t_e} > 0.5\right)$ for 50 nm suspension even though the initial number of 50 nm particles are O (10^3) higher than 860 nm particles. In a static system with large volume, particles can take hours to aggregate.[24,25] However, in droplets, vaporization induced solvent loss leads to a sharp increase in particle loading at some point of the evaporation lifetime ($^t/_{t_e} > 0.5$), thereby triggering rapid agglomeration (Fig. 5).

For 50 nm suspension, particles get deposited near the droplet edge first leading to a coffee ring deposit. Contrarily, in the case of 860 nm suspension, before the particles start accumulating at the contact line, they agglomerate in the solution itself due to high van der Waals force of attraction (Figs. 4 and 5). These agglomerates grow in size with time and can become large enough to exhibit gravimetric induced settling. For a system without any flow, aggregates can sediment if their sizes exceed the critical size[24] given by $R_s = \left(\frac{3kT}{2\pi d\Delta\rho g}\right)^{1/(D+1)}$, where k is the Boltzmann's constant, T is the temperature, d is the nanoparticle diameter, $\Delta\rho$ is difference in particle and solvent densities, g is the acceleration due to gravity, and $D \sim 1.8$ is fractal dimension.[24] Thus, we get $R_s \approx 2\,\mu$m for 860 nm and $\approx 5\,\mu$m for 50 nm suspensions. The corresponding settling velocity as determined from Stokes law is given by $v_s = \frac{g(\rho_p - \rho_l)d_c^{\,2}}{18\mu} \approx 0.1 - 0.6\,\frac{\mu\text{m}}{\text{s}}$, where d_c is the critical particle diameter, ρ_p and ρ_l are the nanoparticle and solvent densities, respectively, and μ is the solvent dynamic viscosity. However, in the present system, recirculating internal flow ($v_i \sim 10\,\mu\text{m/s}$) due to evaporation exhibits velocity magnitude which is two orders higher than v_s. Therefore, for sedimentation to be dominant (to result in uniform deposit), the settling velocity of any aggregate must exceed the flow velocity. The competition between the two velocities can be effectively represented by Peclet number, $Pe = {}^{v_i}/_{v_s}$. Hence, for sedimentation to be dominant, $Pe >= 1$, which results in an effective critical agglomerate size of $d_c = 20\ \mu$m. The flocculates shown in Fig. 5 for 860 nm suspension consist of chains of loosely packed particles (size $\sim 250\,\mu$m; Figs. 5 and 6). The equivalent diameter of the flocculates (single layer) (assuming a single clump of packing density ~ 0.45) is $\sim 25\,\mu$m, which is larger than the critical diameter resulting in Pe > 1. On the other hand, floccules in 50 nm suspension are of the order of $\sim 5\,\mu$m in size (Pe < 1) and do not settle during the evaporation lifetime. Theoretically, for concentrated systems, the critical size required for gelation is given by $R_g = a\varphi^{1/(D-3)}$, where φ is particle concentration when aggregates become visible.[24] Using φ from experimental data (around $^t/_{t_e} > 0.5$), we get $R_g \approx 13\,\mu$m and $\approx 1\,\mu$m for 860 nm and 50 nm suspensions, respectively. This is in correspondence with the experimental

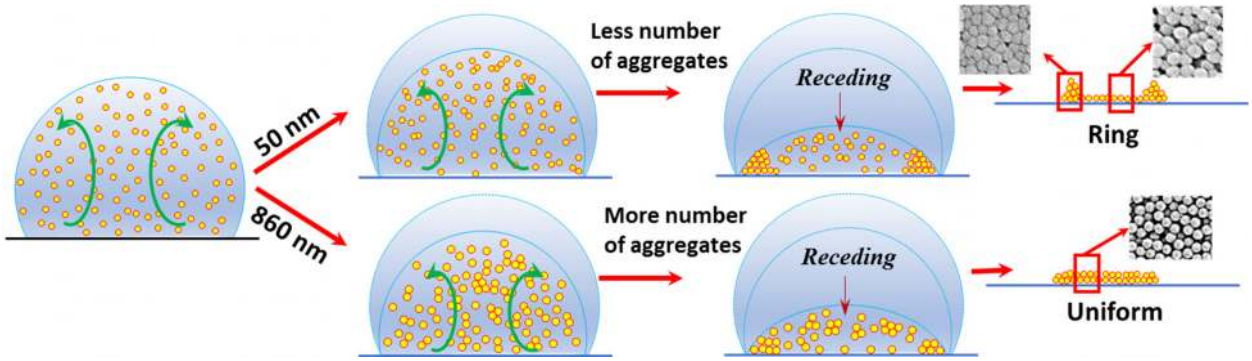

FIG. 4. Schematic showing particle motion and agglomeration leading to the final precipitate. Snapshots correspond to SEM micrographs for the respective condition.

values (similar order). Thus, rapid gravimetric settling ($\mathrm{Pe} > 1$ criterion) along with enhanced particle-substrate attraction within the evaporation timescale are the two reasons responsible for uniform deposits in larger sized nanoparticles.

Particle-particle interactions through agglomeration and settling also alter the self-assembly at the nanoscale, resulting in a spatially varying order to disorder transition. Figure 6 shows the packing order quantified using voronoi reconstruction of the SEM micrograph of the final deposits. For 50 nm suspension, particles are very closely packed [Fig. 6(e)] with a rather large value of the packing fraction of $\sim$0.73. We also observe a large standard deviation (as indicated by width of the peak; Fig. 6) due to order to disorder transition [Fig. 4 inset and Figs. 6(e) and 6(f)] as expected in a typical coffee ring. The packing fraction is therefore quite high near the edge while it is relatively loosely packed towards the droplet center (Fig. 4-inset). On the other hand, particles in 860 nm suspensions are relatively loosely packed with a peak packing fraction $\varphi \sim 0.45$[Figs. 4-inset and 6(a)]. However, even 860 nm suspension exhibits large deviation due to early formation of large floccules (Fig. 5) leading to significant spatial inhomogeneity [Figs. 6(a) and 6(b)]. Intermediate suspensions have packing fraction in-between the two, i.e., $\sim$ 0.52 for 200 and 520 nm suspensions [Figs. 6(d) and 6(c), respectively] with smaller standard deviation. Unlike 50 nm, packing arrangement is same at the center and edges for the remaining particle sizes. Irrespective of the particle size, all the pdfs show bimodal nature. The secondary peaks in the region of lower packing fraction ($\varphi < 0.3$) correspond to intermittent gaps between the particles as can be seen in the inset SEM micrographs in Fig. 6.

In conclusion, we observe a systemic transition from the ring to uniform deposit with the increase in the particle size which cannot be attributed to the internal flow, evaporation modes, and the initial CA. It was found that larger sized nanoparticles undergo rapid agglomeration (with $\mathrm{Pe} > 1$) forming large floccules that undergo gravimetric settling, thereby leading to uniform deposits. In addition, the agglomeration kinetics in turn alters the packing of the particles ranging from loosely packed for 860 nm to very close packing for 50 nm suspensions. Furthermore, the ordering of particles varies in a spatial sense (radially) depending on the particle size exhibiting order to disorder transitions, voids, and grain boundary like features. The resulting uniform deposit can have implications in many applications such as DNA microarrays, thin films, material depositions, etc.

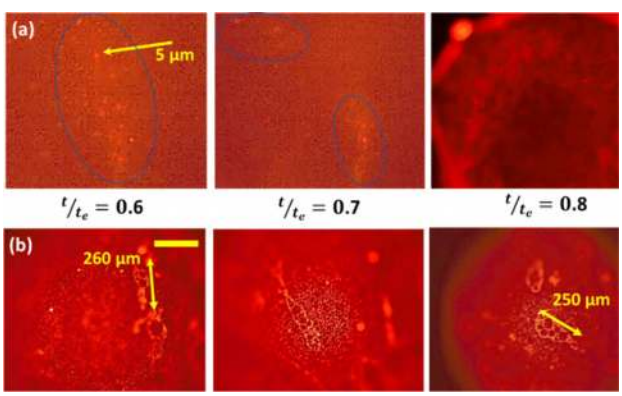

FIG. 5. Fluorescence images of the evaporating droplets showing the agglomerates for (a) 50 nm and (b) 860 nm suspensions. Substrate used is PDMS. Scale bar equals 200 μm. Particle loading rate is 0.01 wt. %. t_e – total evaporation time.

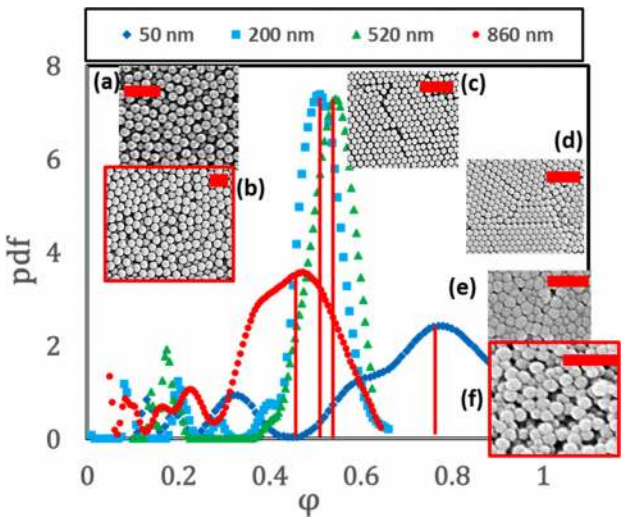

FIG. 6. Probability distribution function of the packing fraction for different packing sizes. Inset: SEM micrographs of the nanoparticles for (a), (b) 860 nm, (c) 520 nm, (d) 200 nm, and (e), (f) 50 nm suspensions. Micrographs in the red boxes correspond to the center of the deposit while others are taken at the deposit edges. Scale bar equals (a) 3.4 μm, (b) 2 μm, (c) 2.6 μm, (d) 1.2 μm, and (e), (f) 200 nm.

See supplementary material for experimental details, snapshots of dried precipitates, and R/R_o graph at lower concentrations and different substrates, fluorescence images, and Table S1 containing initial contact angles for different cases.

[1]B. J. de Gans, P. C. Duineveld, and U. S. Schubert, Adv. Mater. **16**, 203 (2004).
[2]H. Sirringhaus, T. Kawase, R. H. Friend, T. Shimoda, M. Inbasekaran, W. Wu, and E. P. Woo, Science **290**, 2123 (2000).
[3]B. Derby, Annu. Rev. Mater. Res. **40**, 395 (2010).
[4]V. Dugas, J. Broutin, and E. Souteyrand, Langmuir **21**, 9130 (2005).
[5]X. Fang, B. Li, E. Petersen, Y. S. Seo, V. A. Samuilov, Y. Chen, J. C. Sokolov, C. Y. Shew, and M. H. Rafailovich, Langmuir **22**, 6308 (2006).
[6]J. Hou, H. Zhang, Q. Yang, M. Li, Y. Song, and L. Jiang, Angew. Chem., Int. Ed. **53**, 5791 (2014).
[7]X. Kong, Y. Xi, P. LeDuff, E. Li, Y. Liu, L. J. Cheng, G. L. Rorrer, H. Tan, and A. X. Wang, Nanoscale **8**, 17285 (2016).
[8]L. Zhai, M. C. Berg, F. C. Cebeci, Y. Kim, J. M. Milwid, M. F. Rubner, and R. E. Cohen, Nano Lett. **6**, 1213 (2006).
[9]Q. Li, Y. T. Zhu, I. A. Kinloch, and A. H. J. Windle, J. Phys. Chem. B **110**, 13926 (2006).
[10]J. Kim, J. A. Hanna, M. Byun, C. D. Santangelo, and R. C. Hayward, Science **335**, 1201 (2012).
[11]R. D. Deegan, O. Bakajin, T. F. Dupont, G. Huber, S. R. Nagel, and T. A. Witten, Nature **389**, 827 (1997).
[12]P. J. Yunker, T. Still, M. A. Lohr, and A. G. Yodh, Nature **476**, 308 (2011).
[13]Y. Li, Q. Yang, M. Li, and Y. Song, Sci. Rep. **6**, 24628 (2016).
[14]T. Kajiya, W. Kobayashi, T. Okuzono, and M. Doi, J. Phys. Chem. B **113**, 15460 (2009).
[15]T. Still, P. J. Yunker, and A. G. Yodh, Langmuir **28**, 4984 (2012).
[16]H. Hu and R. G. Larson, J. Phys. Chem. B **110**, 7090 (2006).
[17]S. Basu, L. Bansal, and A. Miglani, Soft Matter **12**, 4896 (2016).
[18]A. J. D. Shaikeea, S. Basu, A. Tyagi, S. Sharma, R. Hans, and L. Bansal, PLoS One **12**, e0184997 (2017).
[19]S. Vafaei, T. Borca-Tasciuc, M. Z. Podowski, A. Purkayastha, G. Ramanath, and P. M. Ajayan, Nanotechnology **17**, 2523 (2006).
[20]K. Sefiane, J. Skilling, and J. MacGillivray, Adv. Colloid Interface Sci. **138**, 101 (2008).
[21]D. T. Wasan and A. D. Nikolov, Nature **423**, 156 (2003).
[22]S. Dash, A. Chandramohan, J. A. Weibel, and S. V. Garimella, Phys. Rev. E **90**, 062407 (2014).
[23]J. N. Israelachvili, *Intermolecular and Surface Forces* (Academic Press, 2011).
[24]L. G. Bremer, P. Walstra, and T. van Vliet, Colloids Surf., A **99**, 121 (1995).
[25]Y. J. Yang, A. V. Kelkar, D. S. Corti, and E. I. Franses, Langmuir **32**, 5111 (2016).
[26]L. Bansal, S. Hatte, S. Basu, and S. Chakraborty, Appl. Phys. Lett. **111**, 101601 (2017).
[27]L. Bansal, A. Miglani, and S. Basu, Phys. Rev. E **92**, 042304 (2015).